Journal of Nuclear Materials 386–388 (2009) 515–519

Contents lists available at ScienceDirect

Journal of Nuclear Materials

journal homepage: www.elsevier.com/locate/jnucmat

On the lattice coherency of oxide particles dispersed in EUROFER97

A. Ramar *, N. Baluc, R. Schäublin

Ecole Polytechnique Fédérale de Lausanne (EPFL), Centre de Recherches en Physique des Plasmas, Association Euratom-Confédération Suisse CH 5232 Villigen PSI, Switzerland

A B S T R A C T

Oxide dispersion strengthened steels based on the ferritic/martensitic steel EUROFER97 are developed. The reinforcing particles dispersed in the matrix of EUROFER97 are made of yttria and yttrium titanium oxides. Microstructure is investigated by transmission electron microscopy (TEM). The ODS with yttria presents a tempered martensitic microstructure and a uniform distribution of the yttria. The ODS with yttrium titanium oxide (Y–Ti–O) presents a nano-grained microstructure with a uniform distribution of the Y–Ti–O complex oxides. The microstructure of the yttria particles is investigated by high resolution TEM (HR-TEM). It is found that the dispersed particles made of yttria and Y–Ti oxide are at most semi-coherent with the matrix. The yttria keeps its bcc bulk crystalline structure even after incorporation in EUROFER97.

1. Introduction

Oxide dispersion strengthened (ODS) ferritic/martensitic steels appear to be promising candidates for the future fusion reactor. They would allow in principle for a higher operating temperature of the fusion reactor, which improves its thermal efficiency. Their inherent properties, good thermal conductivity, swelling resistance and low radiation damage accumulation, deriving from the base material, are further enhanced by the presence of a fine dispersion of oxide particles. In effect, their strength remains higher than the base material with increasing temperature [1–3]. Their creep properties are also improved relatively to the base material [4–6]. The ductile-to-brittle transition temperature, however, is increased by the addition of the oxide dispersion [4].

ODS steels are generally produced through powder metallurgy technique which includes ball milling of the matrix with the dispersoid, followed by hot isostatic pressing (HIP) for the final compaction of the alloy [7]. The oxide that is usually selected for the reinforcement is yttria (Y_2O_3), as it is thermodynamically more stable than nitrides and carbides and is one of the most stable oxides [8]. Small amounts of Ti are added in order to refine the dispersion of reinforcing oxide upon re-precipitation during HIP. It forms complex Y–Ti oxide particles with a size ranging from 5 to 10 nm [9]. It appears that a precise control of the chemistry, and in particular the O and Ti content [10–12] but also the C content, is crucial as contamination by foreign elements during the processing has detrimental effects on the mechanical properties of the final product. In earlier studies [8], it was observed in TEM that the resulting microstructure in 0.3 wt% yttria ODS steel is typical of martensite. Some carbides have precipitated in the matrix due to the process of auto-tempering during the cooling following hot isostatic pressing. 10 to 30 nm yttria particles were observed. They appeared to be homogeneously distributed as compared to commercially produced ODS steel with the same composition [8].

In this study, the base material of interest is the ferritic/martensitic steel EUROFER97, containing 8.9 wt% Cr, 1.1 W, 0.47 Mn, 0.2 V, 0.14 Ta, 0.11 C and Fe for the balance. Two alloys with different types of dispersed oxide, one with yttria and another with complex yttrium titanium oxide are considered in this study. The main interest of the study is to understand the structure and the relationship of the lattice of the dispersed yttria and complex yttrium titanium oxide particle with respect to the matrix of EUROFER97.

2. Methodology

Two types of material are considered. There is (1) ODS EUROFER97 with 0.3 wt% Y_2O_3, so-called 'ODS-Yttria', and (2) ODS EUROFER97 with 0.3 wt% Y_2O_3 and 0.3 wt% Ti, so-called 'ODS Ti'. Low energy ball mill is used for mixing the EUROFER97 powder with the yttria and Ti particles. The milled powder is then compacted by HIP. The final product has a density of about 99.95%. All samples were given an initial treatment of austenising at 980 °C for 1 h followed by air cooling and tempering at 780 °C for 1 h followed by air cooling.

In order to perform TEM observations, disks of 1 mm in diameter are punched in the samples and inserted into a 3 mm stainless steel disk to reduce the magnetic effect from the sample in the microscope [17]. The system is glued with a hard epoxy, mechanically polished to about 100 μm and finally thinned to electron transparency using the jet polishing technique, at −2 °C and 21 V using a solution

* Corresponding author. Tel.: +41 56 310 2645.
E-mail address: amuthanramar@gmail.com (A. Ramar).

0022-3115/$ - see front matter © 2009 Published by Elsevier B.V.
doi:10.1016/j.jnucmat.2008.12.137

of 10 vol.% perchloric acid in ethanol. The thinned samples are investigated in a JEOL2010 TEM, which has a LaB_6 gun, a high tilt lens and is operated at 200 kV. X-ray energy dispersive spectrometry (EDS) was used to identify the chemical composition of the oxide particles and the carbides with an Oxford Instr. Si (Li) detector.

Convergent beam diffraction and SAD method was used on the matrix to measure the lattice parameter. Weak beam, for better spatial resolution, was used with a typical condition $\boldsymbol{g}$(4 to 5 g) with $\boldsymbol{g} = \{0\,1\,1\}$, $\boldsymbol{g} = \{2\,0\,0\}$ and $\boldsymbol{g} = \{1\,1\,2\}$. HR-TEM was performed in order to better identify the yttria lattice structure. Initially pure yttria particles were investigated. It was provided as a powder with particle sizes between 20 and 30 nm. TEM sample preparation consisted in dispersing some of the powder over a carbon film supported by a 3 mm Cu grid.

In order to identify the observed yttria structure HR-TEM images of the yttria are simulated, using the EMS programme [18] and matched to the experimental image. The position of the yttrium and the oxygen atoms in the unit cell of yttria are described in detail elsewhere [16] and is used for the TEM image simulation. The HR-TEM simulation conditions are the following. The energy of the incoming electrons is 200 keV, the spherical aberration of our JEOL 2010 microscope is 1.4 mm, the thickness of the sample is from 1 to 10 nm, the defocus from −100 to 100 nm by steps of 5 nm, the defocus spread is 10 nm and the beam convergence is 1 mrad.

3. Results and discussion

In the case of ODS yttria the material presents the typical morphology of tempered martensite in the as received case (Fig. 1(A)). Few chromium carbides, having sizes ranging from 100 to 200 nm, are found. For the samples heat-treated at 800 °C, there is a relatively denser and uniform distribution of chromium carbides ($Cr_{23}C_6$) precipitates [8]. Their size ranges approximately from 100 to 200 nm. The yttria appears as a dispersion of particles with sizes ranging from 10 to 30 nm (Fig. 2(A)). In the case of ODS Ti the material presents the typical morphology of nano sized grained structure with an average grain size of 200 nm with a high dislocation density relative to the as received case (Fig. 1(B)). Few places of the matrix have clean and larger grains with sizes ranging from 1 to 2 μm. The regions with nano-grained structure present a high density of complex yttrium titanium oxide complex oxide particles with a size ranging from 5 to 10 nm (Fig. 2(B)). No chromium carbides were observed in the ODS Ti as like in the case of ODS yttria. The region with the nano-grained structure presents very high density of complex yttrium titanium oxide particle when compared to the region with the grain size of 1–2 μm. They may then hinder the grain growth leading to the observed nanostructured grain morphology.

In both ODS yttria and ODS Ti, in the dark field TEM image (Fig. 2(A) and (B)) only part of the part of the oxides are lit, while others remain darker. The above observations shows that not all particles are oriented in the same direction with respect to each other and to the matrix. This gives a hint that the particles are not fully coherent with respect to the matrix of EUROFER97.

The structural form of Y_2O_3 stable up to near its melting temperature is cubic, has a space group Ia3, is of $(Mn,Fe)_2O_3$ bixbyite type and is known as C-Y_2O_3 or α-Y_2O_3 [13]. Fig. 3(C) shows the structure of the yttria unit cell viewed along the <1 1 1> direction. It has 80 atoms per unit cell and has a lattice parameter of

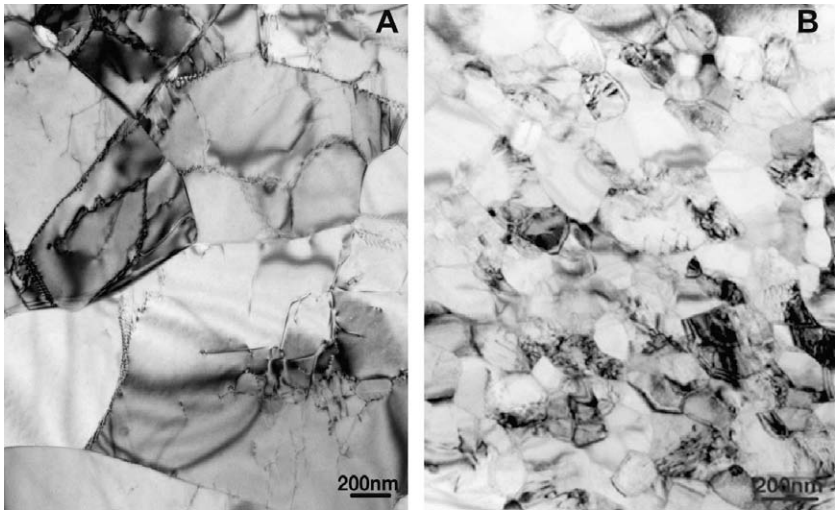

Fig. 1. TEM bright field micrographs showing the microstructure of the alloys in the as received state of (A) ODS yttria and (B) ODS Ti.

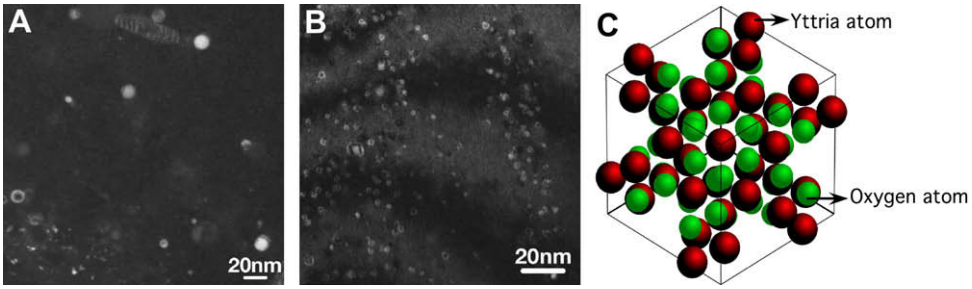

Fig. 2. (A) Yttria and (B) Y–Ti–O particle in the matrix of EUROFER97. (C) Unit cell of the yttria viewed along <1 1 1> direction.

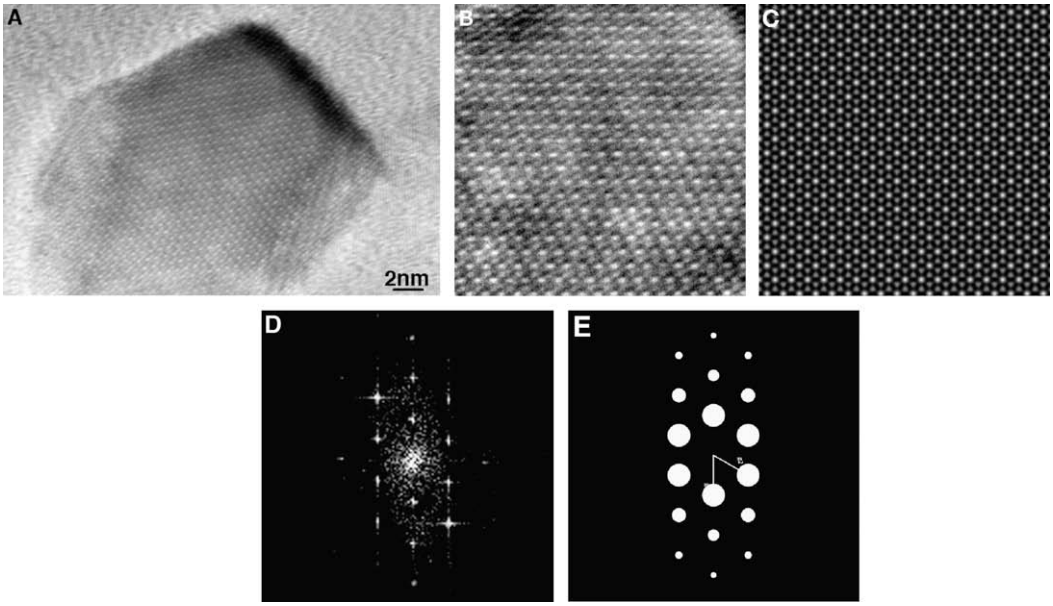

Fig. 3. (A) HR-TEM image of an yttria particle, (B) enlarged image HR-TEM image from (A), (C) simulated HR-TEM image, (D) FFT taken over the image in (B) and (E) simulated diffraction pattern corresponding to the <1 1 1> zone axis.

1.06 nm. The position of the yttrium and the oxygen atoms in the unit cell of yttria are described in detail elsewhere [16]. The crystal structure was also studied by X-ray diffraction and by neutron diffraction [14,15] showing that Y_2O_3 in the latter also exhibits monoclinic C2 space group at high pressures [14]. A transition of *C*-Y_2O_3 to another cubic structure was also observed near 2500 K, when heated by a YAG laser beam. It is a face-centered cubic structure of the fluorite-type, with a space group Fm3m, disordered oxygen vacancies and a room-temperature unit cell parameter of 0.52644 nm [14].

Fig. 3(A) shows a typical HR-TEM image of an yttria particle before dispersion in the matrix of EUROFER97. Fig. 3(B) shows the lattice imaging of the yttria particle derived from Fig. 3(A). Fig. 3(D) shows the power spectrum from the HR-TEM image of the particle (Fig. 3(B)), which is equivalent to a selected area electron diffraction pattern (SAED). The particles are viewed along the zone axis <1 1 1> and the corresponding power spectrum matches perfectly the <1 1 1> diffraction pattern of the yttria structure, as shown in Fig. 3(E). Fig. 3(C) shows the corresponding simulated HR-TEM image of an yttria particle viewed along the <1 1 1> zone axis. There is an excellent match with the experimental image for a defocus of −40 nm and a sample thickness of 5 nm in the simulation.

Fig. 4 shows a region in ODS where the matrix is oriented to <1 0 0> direction. The insert is the corresponding SAED taken over the region. These patterns are characteristic of a bcc structure, relative to fcc and bct, the two other possible phases for this material type. The ferritic nature of the matrix confirms that there is no residual bct structure, which could remain untransformed after tempering. The lattice parameter of the ferritic matrix was determined from the SAED patterns to be 0.294 ± 0.014 nm. There is no observed difference with the one of as received casted EUROFER97.

Fig. 5(A) shows a typical HR-TEM micrograph of the ODS yttria showing one yttria particle in the matrix of EUROFER97. The matrix of the EUROFER97 is oriented along <1 0 0>, as identified from the SAED (Fig. 5(C)). The displayed digital power spectrum (Fig. 5(B)) is obtained in the delineated regions in the yttria particle. The comparison between the power spectrum with the SAED pattern taken in the matrix shows that both the particle and the matrix share a zone axis of <1 0 0>, which hints at some coherency.

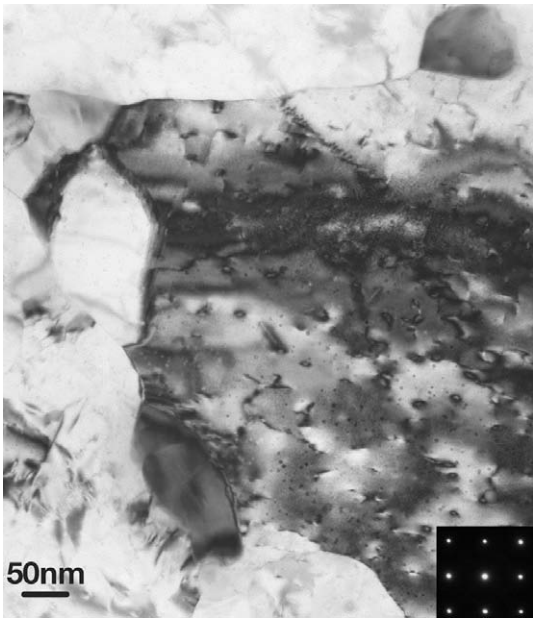

Fig. 4. (a) Bright field TEM micrograph of ODS Yttria oriented along <1 0 0>, insert in the diffraction pattern taken over the matrix.

However, the power spectrum is rotated by about 15° relative to the diffraction pattern, which indicates semi-coherency. The above observations suggest that the yttria particles are some how following the local matrix crystallographic orientation. It occurs during HIPping of the alloy in the austenitic (FCC) phase where the yttria particles embedded in EUROFER97 matrix may have aligned with the matrix lattice tending to full coherency. However due to the difference in the lattice constant and also due to the fast cooling of the alloy, only semi-coherency remains in between the matrix and the yttria particles. Note that, this semi-coherency indicates that the shearing of yttria particles by dislocations will be difficult, leading to hardening.

Fig. 6(A) shows the experimental HR-TEM image of an yttria particle in EUROFER97 matrix viewed along <1 0 0> direction. The

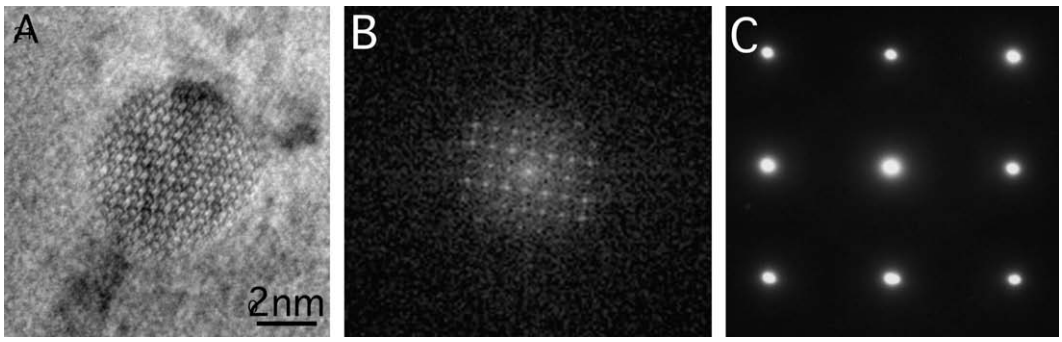

Fig. 5. (A) HR-TEM image showing an yttria particle in EUROFER97 matrix, (B) FFT taken from the particle in the image and (C) diffraction pattern taken in the matrix.

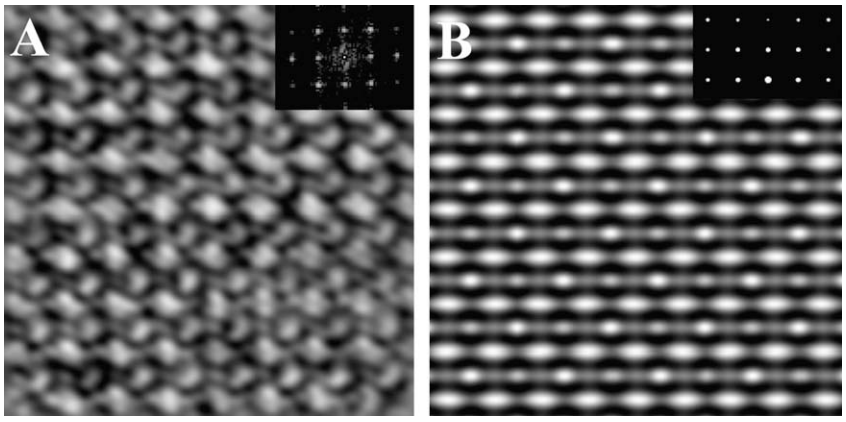

Fig. 6. (A) Experimental HR-TEM image of an yttria particle in EUROFER97 and (B) simulated HR-TEM image of yttria viewed along the <100> direction.

insert is the power spectrum equivalent to the diffraction pattern taken over the HR-TEM image. Fig. 6(B) shows the simulated HR-TEM image of the pure yttria viewed along <100> direction. The insert is the diffraction pattern of the simulated HR-TEM pattern. There is an excellent match of the simulated image with the experimental image in terms of spacing and angle between the white contrast patterns for a defocus of −70 nm and a sample thickness of 7 nm in the simulation. Also, the power spectrum in both cases presents a similar pattern. More preciously, the spacing and angles between the equivalent diffraction spots are the same for the simulated and for the experimental image. These similarities hint at the stability of the structure of the yttria particle before and after incorporation in the matrix. It is thus concluded that ball milling and HIPping do not have any influence on the structure of yttria.

4. Summary and conclusions

The HIPped ODS Yttria and ODS Ti shows the following characteristics,

(1) The ODS Yttria presents tempered martensitic structure in the as received state without any residual bct structure, where as ODS Ti presents nano-grained structure.
(2) The dispersed particles have an average size of 20 nm in the case of ODS yttria, whereas it is about 7 nm in the case of ODS Ti.
(3) The dispersed particles of yttria and complex yttrium titanium oxide are partially coherent with the matrix.
(4) The crystal structure of yttria in the as received powder is bcc, with a lattice parameter of 1.06 nm. There is no change in the yttria crystal structure after getting incorporated in EUROFER97 matrix.

Acknowledgements

This work, supported by the European Communities under the contract of Association between EURATOM/Confédération suisse was carried out within the framework of the European Fusion Development Agreement. The views and opinions expressed herein do not necessarily reflect those of the European Commission. The Paul Scherrer Institute is acknowledged for the overall use of the facilities.

References

[1] D.K. Mukhopadhyay, F.H. Froes, D.S. Gelles, J. Nucl. Mater. 258–263B (1998) 1209.
[2] G.R. Romanoski, L.L. Snead, R.L. Klueh, D.T. Hoelzer, J. Nucl. Mater. 283–287A (2000) 642.
[3] R. Schäublin, T. Leguey, P. Spätig, N. Baluc, M. Victoria, J. Nucl. Mater. 307–311 (2002) 778.
[4] S. Ukai, M. Harada, H. Okada, M. Inoue, S. Nomura, S. Shikakura, K. Asabe, T. Nishida, M. Fujiwara, J. Nucl. Mater. 204 (1993) 65.
[5] V.V. Sagaradze, V.I. Shalaev, V.L. Arbuzov, B.N. Goshchitskii, Yun Tian, Wan Qun, Sun Jiguang, J. Nucl. Mater. 295 (2–3) (2001) 265.
[6] R. Lindau, A. Möslang, M. Schirra, P. Schlossmacher, M. Klimenkov, J. Nucl. Mater. 307–311 (2002) 769.
[7] R. Schäublin, A. Ramar, N. Baluc, V. de Castro, T. Leguey, A. Munoz, N. Schmid, J. Nucl. Mater 351 (2006) 247.
[8] M. Klimiankou, R. Lindau, A. Moslang, J. Cryst. Growth 249 (2003) 381.

[9] S. Ukai, S. Mizuta, M. Fujiwara, T. Okuda, T. Kobayashi, J. Nucl. Sci. Technol. 39 (7) (2002) 778.
[10] S. Ohtsuka, S. Ukai, M. Fujiwara, T. Kaito, T. Narita, J. Nucl. Mater. 329–333 (2004) 372.
[11] S. Ohtsuka, S. Ukai, M. Fujiwara, T. Kaito, T. Narita, J. Phys. Chem. Solids 66 (2005) 571.
[12] C. Cayron, E. Rath, I. Chu, S. Launois, J. Nucl. Mater. 335 (2004) 83.
[13] D. Taylor, Brit. Ceram. Trans. J. 83 (1984) 92.
[14] A.B. Belonoshko, G. Gutierrez, R. Ahuja, B. Johansson, Phys. Rev. B 64 (2001) 184103.
[15] H.R. Hoekstra, K.A. Gingerich, Science 146 (1964) 1163.
[16] M.G. Paton, E.N. Maslen, Acta Cryst. 19 (1965) 307.
[17] R. Schäublin, D. Gelles, M. Victoria, J. Nucl. Mater. 307–311 (2002) 197.
[18] P.A. Stadelmann, Ultramicroscopy 21 (2) (1987) 131.